PERGAMON

International Journal of Solids and Structures 37 (2000) 5329–5351

INTERNATIONAL JOURNAL OF SOLIDS and STRUCTURES

www.elsevier.com/locate/ijsolstr

Three-dimensional Green's functions in anisotropic bimaterials

E. Pan [a], F.G. Yuan [b,*]

[a] *Structures Technology, Inc., Raleigh, NC 27605, USA*
[b] *Department of Mechanical and Aerospace Engineering, North Carolina State University, Raleigh, NC 27695, USA*

Received 12 April 1999; in revised form 24 July 1999

Abstract

In this paper, three-dimensional Green's functions for anisotropic bimaterials are studied based on Stroh formalism and two-dimensional Fourier transforms. Although the Green's functions can be expressed exactly in the Fourier transform domain, it is difficult to obtain the explicit expressions of the Green's functions in the physical domain due to the general anisotropy of the material and a geometry plane involved. Utilizing Fourier inverse transform in the polar coordinate and combining with Mindlin's superposition method, the physical-domain bimaterial Green's functions are derived as a sum of a full-space Green's function and a complementary part. While the full-space Green's function is in an explicit form, the complementary part is expressed in terms of simple regular line-integrals over $[0, 2\pi]$ that are suitable for standard numerical integration. Furthermore, the present bimaterial Green's functions can be reduced to the special cases such as half-space, surface, interfacial, and full-space Green's functions. Numerical examples are given for both half-space and bimaterial cases with isotropic, transversely isotropic, and anisotropic material properties to verify the applicability of the technique. For the half-space case with isotropic or transversely isotropic material properties, the Green's function solutions are in excellent agreement with the existing analytical solutions. For anisotropic half-space and bimaterial cases, numerical results show the strong dependence of the Green's functions on the material properties.

Keywords: Green's functions; Anisotropic bimaterials; Stroh formalism; Fourier transform

1. Introduction

The study of fundamental three-dimensional Green's functions within the context of theory of linear elasticity has been of great interest since the last century. Kelvin (1848) first solved the Green's function

* Corresponding author.

0020-7683/00/$ - see front matter
PII: S0020-7683(99)00216-4

of a point force applied in a full-space isotropic solid. Boussinesq (1885) derived a surface Green's function for a force normal to the free surface in isotropic solids. Mindlin (1936) obtained the half-space Green's function by superposing a complementary part of the solution to the Kelvin's full-space function.

For generally anisotropic solids, Fredholm (1900), Lifshitz and Rozenzweig (1947), Synge (1957), and Mura (1987) have investigated line-integral representations of three-dimensional Green's function in a full-space medium. Recently, explicit expressions for the anisotropic Green's functions were derived by Ting and Lee (1997) in terms of the Stroh eigenvalues (Stroh, 1958, 1962), and by Tonon et al. (1999) based on a formulation of Wang (1997). For the special case of transversely isotropic materials, exact closed-form solutions of the Green's function can be obtained (e.g., Lifshitz and Rozenzweig, 1947; Willis, 1965; Pan and Chou, 1976). The Green's functions of a point force applied in a bimaterial isotropic solid were solved by Rongved (1955) and Dundurs and Hetenyi (1965) with recent work along this line by Fares and Li (1988), Yu and Sanday (1991), Walpole (1996), and Guzina and Pak (1999). It is noted that the general image method presented by Fares and Li (1988) can also be applied to construct the Green's functions in multilayered media (Fares, 1987). The Green's functions in transversely isotropic half-spaces and bimaterials have been developed by Pan and Chou (1979a), (1979b), Yue (1995) and Yu et al. (1995). Actually, by introducing the hexagonal stress vectors, Yu et al. (1995) derived the analytical solutions of the elastic fields due to various defects. Very recently, Liao and co-workers (Liao and Wang, 1998; Wang and Liao, 1999) derived closed-form solutions of the displacements and stresses in a transversely isotropic half-space subjected to various types of loading and applied their results to the analysis of rock mechanics problems. Also, worth mentioning is the work by Gosling and Willis (1994) who derived a line-integral expression for the stresses due to an arbitrary dislocation in an isotropic half-space. For the Green's functions in either an anisotropic half-space or anisotropic bimaterials, a very limited effort has been conducted since Barnett and Lothe (1975) published their classic work. They derived a line-integral expression of the surface Green's function (the displacements on a half-space due to a point force on the free surface) based on Stroh formalism (Barnett and Lothe, 1975). Recently, Walker (1993) derived a Fourier integral expression of the Green's function for an anisotropic half-space, and Qu and Xue (1998) studied the interface crack problems in anisotropic bimaterials using the Stroh formalism. The Stroh formalism in the Radon transformed domain was proposed and applied by Wu (1998) to the three-dimensional anisotropic elasticity where the Green's displacements in an anisotropic half-space due to a point force were obtained in terms of a finite line integral. Also utilizing the Stroh formalism, Ting (1996) derived the anisotropic Green's functions of a point force in a half-space and bimaterials in the Fourier transformed domain, and Yuan and Yang (1999) the transformed-domain Green's functions for multilayered generally anisotropic solids. Although the Green's functions in the physical domain can be calculated through numerical means such as Fast Fourier Transform, the accuracy of the solutions remain doubtful due to the infinite numerical integral and the singular kernels involved.

In this paper, three-dimensional Green's functions of point forces in anisotropic bimaterials by using the Stroh formalism and two-dimensional Fourier transforms are studied. First, the Green's functions in the Fourier transformed domain derived by Ting (1996) and Yuan and Yang (1999) are briefly reviewed and are extended to include the in-plane stress components. Some features related to the transformed-domain Green's functions are also discussed. Secondly, inverse transform in terms of a polar coordinate transform is introduced so that the integral with respect to the radial direction can be performed analytically. Thus, in the physical domain, the Green's functions can be represented in terms of a line-integral. In order to treat the singularities involved, the bimaterial Green's functions are expressed as a sum of a full-space Green's function and a complementary part. This approach is similar to Mindlin's superposition method (Mindlin, 1936) and is particularly beneficial when dealing with anisotropic bimaterial Green's functions. As will be observed below that in doing so, the singularities involved

appear only in the full-space Green's function and they can be easily evaluated using its *explicit* form (Ting and Lee, 1997; Tonon et al., 1999). In addition, the complementary part of the physical-domain Green's functions is expressed in such a way that their derivatives with respect to either the source or field point can be carried out exactly under the regular line-integral. The radial dependence of the complementary part of the Green's functions on the field and source points also resembles those of the corresponding full-space Green's functions. The present bimaterial Green's functions can be reduced to the special cases such as half-space, surface, interfacial, and full-space Green's functions. Furthermore, the present surface Green's displacements can be reduced to the same expression obtained by Barnett and Lothe (1975) or recently by Wu (1998).

Numerical examples are given for both half-space and bimaterial cases with isotropic, transversely isotropic, and anisotropic material properties. For the half-space case with isotropic or transversely isotropic material properties, the current Green's function solutions provide excellent agreement with the existing analytical solutions. For the anisotropic case, the Green's functions in a half-space or in bimaterials show clearly the effect of material anisotropy on the displacement and stress distributions.

2. Problem description

Consider an anisotropic bimaterial full-space where $x_3 > 0$ and $x_3 < 0$ are occupied by materials 1 and 2, respectively (Fig. 1), with the interface being at $x_3 = 0$ plane. Without loss of generality, we assume that a concentrated force $\boldsymbol{f} = (f_1, f_2, f_3)$ is applied at (0, 0, d) in material 1 with $d > 0$. The problem domain may be artificially divided into three regions: $x_3 > d$ (in material 1), $0 \leq x_3 < d$ (in material 1), and $x_3 < 0$ (in material 2).

In these regions, the equations of equilibrium in terms of displacements u_k in the absence of body forces are written as

$$C_{ijkl} u_{k,\,lj} = 0 \tag{1}$$

where C_{ijkl} is the elastic stiffness tensor of the corresponding region.

The boundary conditions at the interface $x_3 = 0$ require that the displacement and traction vectors are continuous, i.e.,

$$\boldsymbol{u}_1|_{x_3=0^+} = \boldsymbol{u}_2|_{x_3=0^-}, \qquad \boldsymbol{t}_1|_{x_3=0^+} = \boldsymbol{t}_2|_{x_3=0^-} \tag{2}$$

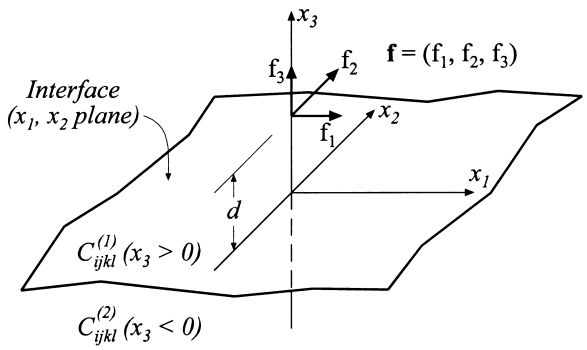

Fig. 1. An anisotropic bimaterial full-space subjected to a concentrated force $\boldsymbol{f}$ applied at (0, 0, d) in material 1.

where $\boldsymbol{t}_1$ and $\boldsymbol{t}_2$ are, respectively, the traction vectors on x_3 = constant plane with components defined as

$$\boldsymbol{t} = (\boldsymbol{\sigma}_{13}, \boldsymbol{\sigma}_{23}, \boldsymbol{\sigma}_{33}) \tag{3}$$

At the plane $x_3 = d$ where the point force is applied, the displacement and traction vectors satisfy the following conditions

$$\boldsymbol{u}_1|_{x_3=d^-} = \boldsymbol{u}_1|_{x_3=d^+}$$

$$\boldsymbol{t}_1|_{x_3=d^-} - \boldsymbol{t}_1|_{x_3=d^+} = \delta(x_1)\delta(x_2)\boldsymbol{f} \tag{4}$$

Apart from these conditions, the solutions in the region of $x_3 > d$ in material 1, and in the region of $x_3 < 0$ in material 2 are required to be bounded as x_3 approaches $+\infty$ and $-\infty$, respectively.

3. General solutions in the transformed domain

To solve the problem described in the previous section, the two-dimensional Fourier transforms

$$\tilde{u}_k(y_1, y_2, x_3) = \int\int u_k(x_1, x_2, x_3)\mathrm{e}^{i\boldsymbol{y}\cdot\boldsymbol{x}}\,\mathrm{d}x_1\,\mathrm{d}x_2 \tag{5}$$

are applied. In Eq. (5), $\boldsymbol{y} = (y_1, y_2)$ is the transform vector; $\boldsymbol{x}$ denotes (x_1, x_2), and

$$\boldsymbol{y}\cdot\boldsymbol{x} = y_1x_1 + y_2x_2$$

In the transformed domain, Eq. (1) becomes

$$C_{i\alpha k\beta} + y_\alpha y_\beta \tilde{u}_k + i(C_{i\alpha k3} + C_{i3k\alpha})y_\alpha \tilde{u}_{k,3} - C_{i3k3}\tilde{u}_{k,33} = 0 \tag{6}$$

where $\alpha, \beta = 1, 2$. Now, letting

$$\boldsymbol{y} = \eta\boldsymbol{n}, \quad \boldsymbol{n} = \begin{bmatrix} n_1 \\ n_2 \\ 0 \end{bmatrix} = \begin{bmatrix} \cos\theta \\ \sin\theta \\ 0 \end{bmatrix}, \quad \boldsymbol{m} = \begin{bmatrix} 0 \\ 0 \\ 1 \end{bmatrix} \tag{7}$$

a general solution of Eq. (6) can then be expressed as

$$\tilde{\boldsymbol{u}}(y_1, y_2, x_3) = \boldsymbol{a}\,\mathrm{e}^{-ip\eta x_3} \tag{8}$$

with p and $\boldsymbol{a}$ satisfying the following eigenrelation:

$$\left[\boldsymbol{Q} + p\left(\boldsymbol{R} + \boldsymbol{R}^{\mathrm{T}}\right) + p^2\boldsymbol{T}\right]\boldsymbol{a} = 0 \tag{9}$$

where

$$Q_{ik} = C_{ijks}n_jn_s, \quad R_{ik} = C_{ijks}n_jm_s, \quad T_{ik} = C_{ijks}m_jm_s \tag{10}$$

In Eq. (9), the superscript T denotes the transpose. It has been shown (Eshelby et al., 1953; Ting, 1996) that the eigenvalues of Eq. (9) are either complex or purely imaginary by the positive strain energy density requirement. It is also noted that Eq. (9) is the Stroh eigenrelation for the oblique plane spanned

by $\boldsymbol{n}$ and $\boldsymbol{m}$ defined in Eq. (7). The traction vector $\boldsymbol{t}$ on the x_3 = constant plane and the in-plane stress vector $\boldsymbol{s}$ are related to the displacements as

$$\boldsymbol{t} \equiv (\boldsymbol{\sigma}_{13}, \boldsymbol{\sigma}_{23}, \boldsymbol{\sigma}_{33}) = \left(C_{13kl}u_{k,\,l}, C_{23kl}u_{k,\,l}, C_{33kl}u_{k,\,l}\right) \tag{11}$$

$$\boldsymbol{s} \equiv (\boldsymbol{\sigma}_{11}, \boldsymbol{\sigma}_{12}, \boldsymbol{\sigma}_{22}) = \left(C_{11kl}u_{k,\,l}, C_{12kl}u_{k,\,l}, C_{22kl}u_{k,\,l}\right) \tag{12}$$

Using the displacement solution (8), the transformed traction and in-plane stress vectors can be found as

$$\tilde{\boldsymbol{t}} = -i\eta\boldsymbol{b}\ \mathrm{e}^{-ip\eta x_3} \tag{13}$$

$$\tilde{\boldsymbol{s}} = -i\eta\boldsymbol{c}\ \mathrm{e}^{-ip\eta x_3} \tag{14}$$

with

$$\boldsymbol{b} = \left(\boldsymbol{R}^{\mathrm{T}} + p\boldsymbol{T}\right)\boldsymbol{a} = -\frac{1}{p}(\boldsymbol{Q} + p\boldsymbol{R})\boldsymbol{a}$$

$$\boldsymbol{c} = \boldsymbol{D}\boldsymbol{a} \tag{15}$$

where the matrix $\boldsymbol{D}$ is defined by

$$\boldsymbol{D} = \begin{bmatrix} C_{111\alpha}n_\alpha + pC_{1113} & C_{112\alpha}n_\alpha + pC_{1123} & C_{113\alpha}n_\alpha + pC_{1133} \\ C_{121\alpha}n_\alpha + pC_{1213} & C_{122\alpha}n_\alpha + pC_{1223} & C_{123\alpha}n_\alpha + pC_{1233} \\ C_{221\alpha}n_\alpha + pC_{2213} & C_{222\alpha}n_\alpha + pC_{2223} & C_{223\alpha}n_\alpha + pC_{2233} \end{bmatrix} \tag{16}$$

If p_j, a_j, and b_j (j = 1, 2,…,6) are the eigenvalues and the associated eigenvectors, we let

$$\mathrm{Im}\, p_j > 0, \quad p_{j+3} = \bar{p}_j, \quad \boldsymbol{a}_{j+3} = \bar{\boldsymbol{a}}_j, \quad \boldsymbol{b}_{j+3} = \bar{\boldsymbol{b}}_j, \quad \boldsymbol{c}_{j+3} = \bar{\boldsymbol{c}}_j, \quad (j = 1, 2, 3)$$

$$\boldsymbol{A} = [\boldsymbol{a}_1, \boldsymbol{a}_2, \boldsymbol{a}_3] \quad \boldsymbol{B} = \left[\boldsymbol{b}_1, \boldsymbol{b}_{2;}, \boldsymbol{b}_3\right], \quad \boldsymbol{C} = [\boldsymbol{c}_1, \boldsymbol{c}_2, \boldsymbol{c}_3] \tag{17}$$

where 'Im' stands for the imaginary part and the overbar denotes the complex conjugate.

Assuming that p_α are distinct, and the eigenvectors a_j, and b_j satisfy the following normalization relation

$$\boldsymbol{b}_i^{\mathrm{T}}\boldsymbol{a}_j + \boldsymbol{a}_i^{\mathrm{T}}\boldsymbol{b}_j = \delta_{ij} \tag{18}$$

with δ_{ij} being the Kronecker delta, then the general solutions of Eq. (6) in the transformed domain can be obtained by superposing six eigensolutions of Eq. (8) (Yuan and Yang, 1999), that is

$$\tilde{\boldsymbol{u}}(y_1, y_2, x_3) = i\eta^{-1}\bar{\boldsymbol{A}} < \mathrm{e}^{-i\bar{p}_*\eta x_3} > \bar{\boldsymbol{q}} + i\eta^{-1}\boldsymbol{A} < \mathrm{e}^{-ip_*\eta x_3} > \boldsymbol{q}'$$

$$\tilde{\boldsymbol{t}}(y_1, y_2, x_3) = \bar{\boldsymbol{B}} < \mathrm{e}^{-i\bar{p}_*\eta x_3} > \bar{\boldsymbol{q}} + \boldsymbol{B} < \mathrm{e}^{-ip_*\eta x_3} > \boldsymbol{q}'$$

$$\tilde{\boldsymbol{s}}(y_1, y_2, x_3) = \bar{\boldsymbol{C}} < \mathrm{e}^{-i\bar{p}_*\eta x_3} > \bar{\boldsymbol{q}} + \boldsymbol{C} < \mathrm{e}^{-ip_*\eta x_3} > \boldsymbol{q}' \tag{19}$$

where $\bar{\boldsymbol{q}}$and $\boldsymbol{q}'$ are arbitrary complex vectors to be determined and

$$\langle \mathrm{e}^{-ip_*\eta x_3}\rangle = \mathrm{diag}\left[\mathrm{e}^{-ip_1\eta x_3}, \mathrm{e}^{-ip_2\eta x_3}, \mathrm{e}^{-ip_3\eta x_3}\right] \tag{20}$$

It is also worth mentioning that the general solutions (19) remain valid if x_3 is replaced by $(x_3-\gamma)$ with γ being an arbitrary real constant. In addition, besides their obvious dependence on material properties, the matrices $\boldsymbol{A}$, $\boldsymbol{B}$, $\boldsymbol{C}$, vectors $\bar{\boldsymbol{q}}$, $\boldsymbol{q}'$, and p_j are also functions of the unit vector $\boldsymbol{n}$.

4. Bimaterial Green's functions in the transformed domain

For the anisotropic bimaterials, the continuity condition in Eq. (2) at the interface $x_3=0$ and the condition (4) at $x_3=d$ become, in the transformed domain, as

$$\tilde{\boldsymbol{u}}_1|_{x_3=0^+} = \tilde{\boldsymbol{u}}_2|_{x_3=0^-}, \qquad \tilde{\boldsymbol{t}}_1|_{x_3=0^+} = \tilde{\boldsymbol{t}}_2|_{x_3=0^-} \tag{21}$$

and

$$\tilde{\boldsymbol{u}}_1|_{x_3=d^-} = \tilde{\boldsymbol{u}}_1|_{x_3=d^+}$$

$$\tilde{\boldsymbol{t}}_1|_{x_3=d^-} - \tilde{\boldsymbol{t}}_1|_{x_3=d^+} = \boldsymbol{f} \tag{22}$$

Using these conditions as well as the requirement that the solutions should be bounded as x_3 approaches infinity, the bimaterial Green's functions in the transformed domain can be derived as (Yuan and Yang, 1999)

For $x_3 > d$ (in material 1)

$$\tilde{\boldsymbol{u}}_1(y_1,y_2,x_3), = -i\eta^{-1}\bar{\boldsymbol{A}}_1\langle \mathrm{e}^{-i\bar{p}_*^{(1)}\eta(x_3-d)}\rangle\bar{\boldsymbol{q}}_1^{\infty} - i\eta^{-1}\bar{\boldsymbol{A}}_1\langle \mathrm{e}^{-i\bar{p}_*^{(1)}\eta x_3}\rangle\bar{\boldsymbol{q}}_1$$

$$\tilde{\boldsymbol{t}}_1(y_1,y_2,x_3) = -\bar{\boldsymbol{B}}_1\langle \mathrm{e}^{-i\bar{p}_*^{(1)}\eta(x_3-d)}\rangle\bar{\boldsymbol{q}}_1^{\infty} - \bar{\boldsymbol{B}}_1\langle \mathrm{e}^{-i\bar{p}_*^{(1)}\eta x_3}\rangle\bar{\boldsymbol{q}}_1$$

$$\tilde{\boldsymbol{s}}_1(y_1,y_2,x_3) = -\bar{\boldsymbol{C}}_1\langle \mathrm{e}^{-i\bar{p}_*^{(1)}\eta(x_3-d)}\rangle\bar{\boldsymbol{q}}_1^{\infty} - \bar{\boldsymbol{C}}_1\langle \mathrm{e}^{-i\bar{p}_*^{(1)}\eta x_3}\rangle\bar{\boldsymbol{q}}_1 \tag{23}$$

For $0 \le x_3 < d$ (in material 1)

$$\tilde{\boldsymbol{u}}_1(y_1,y_2,x_3) = i\eta^{-1}\boldsymbol{A}_1\langle \mathrm{e}^{-ip_*^{(1)}\eta(x_3-d)}\rangle\boldsymbol{q}_1^{\infty} - i\eta^{-1}\bar{\boldsymbol{A}}_1\langle \mathrm{e}^{-i\bar{p}_*^{(1)}\eta x_3}\rangle\bar{\boldsymbol{q}}_1$$

$$\tilde{\boldsymbol{t}}_1(y_1,y_2,x_3) = \boldsymbol{B}_1\langle \mathrm{e}^{-ip_*^{(1)}\eta(x_3-d)}\rangle\boldsymbol{q}_1^{\infty} - \bar{\boldsymbol{B}}_1\langle \mathrm{e}^{-i\bar{p}_*^{(1)}\eta x_3}\rangle\bar{\boldsymbol{q}}_1$$

$$\tilde{\boldsymbol{s}}_1(y_1,y_2,x_3) = \boldsymbol{C}_1\langle \mathrm{e}^{-ip_*^{(1)}\eta(x_3-d)}\rangle\boldsymbol{q}_1^{\infty} - \bar{\boldsymbol{C}}_1\langle \mathrm{e}^{-i\bar{p}_*^{(1)}\eta x_3}\rangle\bar{\boldsymbol{q}}_1 \tag{24}$$

For $x_3 < 0$ (in material 2)

$$\tilde{\boldsymbol{u}}_2(y_1,y_2,x_3) = i\eta^{-1}\boldsymbol{A}_2\langle \mathrm{e}^{-ip_*^{(2)}\eta x_3}\rangle\boldsymbol{q}_2$$

$$\tilde{\boldsymbol{t}}_2(y_1, y_2, x_3) = \boldsymbol{B}_2\langle \mathrm{e}^{-ip_*^{(2)}\eta x_3}\rangle \boldsymbol{q}_2$$

$$\tilde{\boldsymbol{s}}_2(y_1, y_2, x_3) = \boldsymbol{C}_2\langle \mathrm{e}^{-ip_*^{(2)}\eta x_3}\rangle \boldsymbol{q}_2 \tag{25}$$

where subscripts 1 and 2 denote the quantities in materials 1 and 2, respectively and

$$\boldsymbol{q}_1^{\infty} = \boldsymbol{A}_1^{\mathrm{T}}\boldsymbol{f} \tag{26}$$

The complex vectors $\bar{\boldsymbol{q}}_1$ and $\boldsymbol{q}_2$ in Eqs. (23)–(25) are determined by

$$\bar{\boldsymbol{q}}_1 = \boldsymbol{G}_1\langle \mathrm{e}^{ip_*^{(1)}\eta d}\rangle \boldsymbol{A}_1^{\mathrm{T}}\boldsymbol{f} \tag{27a}$$

$$\boldsymbol{q}_2 = \boldsymbol{G}_2\langle \mathrm{e}^{ip_*^{(1)}\eta d}\rangle \boldsymbol{A}_1^{\mathrm{T}}\boldsymbol{f} \tag{27b}$$

$$\boldsymbol{G}_1 = -\bar{\boldsymbol{A}}_1^{-1}\left(\bar{\boldsymbol{M}}_1 + \boldsymbol{M}_2\right)^{-1}(\boldsymbol{M}_1 - \boldsymbol{M}_2)\boldsymbol{A}_1$$

$$\boldsymbol{G}_2 = \boldsymbol{A}_2^{-1}\left(\bar{\boldsymbol{M}}_1 + \boldsymbol{M}_2\right)^{-1}\left(\boldsymbol{M}_1 + \bar{\boldsymbol{M}}_1\right)\boldsymbol{A}_1 \tag{28}$$

where $\boldsymbol{M}_\alpha$ are the impedance tensors defined as

$$\boldsymbol{M}_\alpha = -i\boldsymbol{B}_\alpha\boldsymbol{A}_\alpha^{-1} \quad (\alpha = 1, 2) \tag{29}$$

Eqs. (23)–(25) are the bimaterial Green's displacements and stresses in the Fourier transformed domain. Several important features pertained to these Green's functions are highlighted below:

1. For the solutions in material 1 ($x_3 > 0$), the first terms in Eqs. (23) and (24) are the transformed-domain Green's function for the anisotropic full-space. The inverse of this Green's function, i.e., the physical-domain solutions, has been developed recently by Ting and Lee (1997) and Tonon et al. (1999) in an explicit form. Therefore, the Fourier inverse transform needs to be carried out only for the second terms of the solutions, which are similar to the complementary part of the Mindlin's solution (Mindlin, 1936). This observation is critical in that the singularities involved in the physical-domain bimaterial Green's function actually appear only in the full-space Green's function. Since the latter function has an explicit-form representation, such singularities can be evaluated easily. Thus, the complementary part of the bimaterial Green's function is regular everywhere in its assigned region with the only exception of $x_3 = d = 0$. This special case will be addressed in Appendix A.
2. When the material properties in materials 1 and 2 are identical, $\boldsymbol{G}_1 = \boldsymbol{0}$ and $\boldsymbol{G}_2 = \boldsymbol{I}$, the expressions of the coefficients in Eqs. (27a) and (27b) are reduced to

$$\bar{\boldsymbol{q}}_1 = \boldsymbol{0}$$

$$\boldsymbol{q}_2 = \langle \mathrm{e}^{ip_*^{(1)}\eta d}\rangle \boldsymbol{A}_1^{\mathrm{T}}\boldsymbol{f} \tag{30}$$

   Thus, the bimaterial Green's functions are reduced automatically to the solutions in the full-space.
3. When $d \to 0^+$, the solutions in the region $0 \le x_3 < d$ disappear, and the remaining Green's functions are reduced to the interfacial Green's functions with a point force applied at the interface of material 1.
4. Eqs. (23)–(25) can also be reduced to the half-space Green's functions by ignoring Eq. (25) (i.e., solutions in material 2) and letting $\boldsymbol{B}_2 = \boldsymbol{0}$. In this case, $\boldsymbol{G}_1$ in Eq. (28) is simplified to

$$\boldsymbol{G}_1 = \bar{\boldsymbol{B}}_1^{-1}\boldsymbol{B}_1 \tag{31}$$

5. Bimaterial Green's functions in the physical domain

Having obtained the Green's functions in the transformed domain, we now apply the inverse Fourier transform to Eqs. (23)–(25). To handle the double infinite integrals, the polar coordinate transform is introduced so that the infinite integral with respect to the radial variable can be carried out exactly. Thus, the final bimaterial Green's functions in the physical domain can be expressed in terms of a regular line-integral over $[0, 2\pi]$. In the following, we will use only the displacement solution in region $x_3 > d$ of material 1 to illustrate the derivation, and list the final results for other Green's functions.

Applying the Fourier inverse transform, the Green's displacement in Eq. (23) gives

$$\boldsymbol{u}_1(x_1, x_2, x_3) = -\frac{i}{4\pi^2}\int\int\left\{\eta^{-1}\bar{\boldsymbol{A}}_1\langle \mathrm{e}^{-i\bar{p}_*^{(1)}\eta(x_3-d)}\rangle\bar{\boldsymbol{q}}_1^{\infty}\,\mathrm{e}^{-i(x_1y_1+x_2y_2)}\right\}\mathrm{d}y_1\,\mathrm{d}y_2$$

$$-\frac{i}{4\pi^2}\int\int\left\{\eta^{-1}\bar{\boldsymbol{A}}_1\langle \mathrm{e}^{-i\bar{p}_*^{(1)}\eta x_3}\rangle\bar{\boldsymbol{q}}_1\,\mathrm{e}^{-i(x_1y_1+x_2y_2)}\right\}\mathrm{d}y_1\,\mathrm{d}y_2 \tag{32}$$

The first integral in Eq. (32) corresponds to the full-space Green's displacement that is available in an explicit form (Ting and Lee, 1997; Tonon et al., 1999). Consequently, the inverse transform needs to be carried out only for the second regular integral, or the complementary part. The singularities involved in the bimaterial Green's function appear only in the full-space solution that can be evaluated easily because of its explicit-form expression. Denoting the full-space Green's function by $\boldsymbol{u}_1^{\infty}(x_1, x_2, x_3)$ and introducing a polar coordinate transform consistent with the one defined in Eq. (7), i.e.,

$$y_1 = \eta\cos\theta$$

$$y_2 = \eta\sin\theta \tag{33}$$

Then, Eq. (32), also with use of (27a), become

$$\boldsymbol{u}_1(x_1, x_2, x_3) = \boldsymbol{u}_1^{\infty}(x_1, x_2, x_3)$$

$$-\frac{i}{4\pi^2}\left[\int_0^{2\pi}\mathrm{d}\theta\int_0^{\infty}\bar{\boldsymbol{A}}_1\langle \mathrm{e}^{-i\bar{p}_*^{(1)}\eta x_3}\rangle\boldsymbol{G}_1\langle \mathrm{e}^{ip_*^{(1)}\eta d}\rangle\mathrm{e}^{-i\eta(x_1\cos\theta+x_2\sin\theta)}\boldsymbol{A}_1^{\mathrm{T}}\,\mathrm{d}\eta\right]\boldsymbol{f} \tag{34}$$

Since the matrices $\boldsymbol{A}_1$ and $\boldsymbol{G}_1$ are independent of the radial variable η, the integral with respect to η can actually be performed analytically. Assuming that $x_3 \neq 0$ or $d \neq 0$, Eq. (34) can be reduced to a compact form

$$\boldsymbol{u}_1(x_1, x_2, x_3) = \boldsymbol{u}_1^{\infty}(x_1, x_2, x_3) + \frac{1}{4\pi^2}\left[\int_0^{2\pi}\bar{\boldsymbol{A}}_1\boldsymbol{G}_u^{(1)}\boldsymbol{A}_1^{\mathrm{T}}\,\mathrm{d}\theta\right]\boldsymbol{f} \tag{35}$$

where

$$\left(\boldsymbol{G}_u^{(1)}\right)_{ij} = \frac{(\boldsymbol{G}_1)_{ij}}{-\bar{p}_i^{(1)} x_3 + p_j^{(1)} d - (x_1 \cos\theta + x_2 \sin\theta)} \tag{36}$$

Using a similar procedure, other bimaterial Green's functions can be derived and the results are listed below:

$$\begin{aligned}
\boldsymbol{t}_1(x_1, x_2, x_3) &= \boldsymbol{t}_1^{\infty}(x_1, x_2, x_3) + \frac{1}{4\pi^2}\left[\int_0^{2\pi} \bar{\boldsymbol{B}}_1 \boldsymbol{G}_t^{(1)} \boldsymbol{A}_1^{\mathrm{T}}\, \mathrm{d}\theta\right]\boldsymbol{f} \\
\boldsymbol{s}_1(x_1, x_2, x_3) &= \boldsymbol{s}_1^{\infty}(x_1, x_2, x_3) + \frac{1}{4\pi^2}\left[\int_0^{2\pi} \bar{\boldsymbol{C}}_1 \boldsymbol{G}_t^{(1)} \boldsymbol{A}_1^{\mathrm{T}}\, \mathrm{d}\theta\right]\boldsymbol{f} \\
\boldsymbol{u}_2(x_1, x_2, x_3) &= -\frac{1}{4\pi^2}\left[\int_0^{2\pi} \boldsymbol{A}_2 \boldsymbol{G}_u^{(2)} \boldsymbol{A}_1^{\mathrm{T}}\, \mathrm{d}\theta\right]\boldsymbol{f} \\
\boldsymbol{t}_2(x_1, x_2, x_3) &= -\frac{1}{4\pi^2}\left[\int_0^{2\pi} \boldsymbol{B}_2 \boldsymbol{G}_t^{(2)} \boldsymbol{A}_1^{\mathrm{T}}\, \mathrm{d}\theta\right]\boldsymbol{f} \\
\boldsymbol{s}_2(x_1, x_2, x_3) &= -\frac{1}{4\pi^2}\left[\int_0^{2\pi} \boldsymbol{C}_2 \boldsymbol{G}_t^{(2)} \boldsymbol{A}_1^{\mathrm{T}}\, \mathrm{d}\theta\right]\boldsymbol{f}
\end{aligned} \tag{37, 38}$$

In Eqs. (37) and (38), $\boldsymbol{t}_1^{\infty}(x_1, x_2, x_3)$ and $\boldsymbol{s}_1^{\infty}(x_1, x_2, x_3)$ are the Green's stresses in the full-space and

$$\left(\boldsymbol{G}_t^{(1)}\right)_{ij} = \frac{(\boldsymbol{G}_1)_{ij}}{\left[-\bar{p}_i^{(1)} x_3 + p_j^{(1)} d - (x_1 \cos\theta + x_2 \sin\theta)\right]^2} \tag{39}$$

$$\left(\boldsymbol{G}_u^{(2)}\right)_{ij} = \frac{(\boldsymbol{G}_2)_{ij}}{-p_i^{(2)} x_3 + p_j^{(1)} d - (x_1 \cos\theta + x_2 \sin\theta)} \tag{40}$$

$$\left(\boldsymbol{G}_t^{(2)}\right)_{ij} = \frac{(\boldsymbol{G}_2)_{ij}}{\left[-p_i^{(2)} x_3 + p_j^{(1)} d - (x_1 \cos\theta + x_2 \sin\theta)\right]^2} \tag{41}$$

Therefore, the complementary part of the bimaterial Green's displacements and stresses can be expressed in terms of a regular line integral over $[0, 2\pi]$. With regard to these physical-domain bimaterial Green's functions (Eqs. (35), (37), and (38)), the following important observations can be made:

1. In deriving the results, we have assumed that the point force (source point) is located at $(0, 0, d)$. For a force located at (x_1^0, x_2^0, d), the variables x_1 and x_2 in the above expressions need to be replaced by $x_1 - x_1^0$ and $x_2 - x_2^0$, respectively.
2. Similar to the procedures made on the transformed-domain Green's functions, the physical-domain

Table 1
Green's functions results in an isotropic half-space

$\boldsymbol{u}/(f/Ed)$	$S(0, 0, d)$, $F(0, 0, 0.75d)$		$S(0, 0, d)$, $F(0, 0, 1.25d)$	
	Present	Mindlin (1936)	Present	Mindlin (1936)
(1, 1) = (2, 2)	0.618598	0.618584	0.599496	0.599482
(3, 3)	1.034496	1.034490	0.988784	0.988780
$\boldsymbol{\sigma}/(f/d^2)$				
(1, 5) = (2, 4)	0.335471	0.335450	−0.379938	−0.379918
(3, 1) = (3, 2)	−0.397176	−0.397176	0.352272	0.352272
(3, 3)	2.961820	2.961776	−3.173624	−3.173576

Green's functions presented here can be reduced to the half-space, interfacial, and homogeneous Green's functions by a suitable substitution of the involved vectors and matrices.

3. For the complementary part of the solution in material 1 and the solution in material 2, the dependence of the solutions on the field point (x_1, x_2, x_3) and source point (x_1^0, x_2^0, d) appears only through matrices $\boldsymbol{G}_u^{(1)}$, $\boldsymbol{G}_t^{(1)}$, $\boldsymbol{G}_u^{(2)}$, and $\boldsymbol{G}_t^{(2)}$ as defined in Eqs. (36) and (39)–(41). Therefore, the derivatives of the bimaterial Green's functions with respect to either the field or source point can be exactly carried out under the integral sign. These derivatives are required in the integral equation method for the internal stress and fracture analyses in bimaterial solids.
4. The bimaterial Green's functions for displacements and stresses are inversely proportional to, respectively, a linear and quadratic combination of the field and source coordinates. These features resemble the behavior of the full-space Green's displacement ($\propto 1/r$) and stress ($\propto 1/r^2$) where r is the distance between the source and field points.
5. The integrals in Eqs. (35), (37), and (38) for performing the complementary part of the Green's functions are regular and thus can be easily carried out by a standard numerical integral method such as the Gauss quadrature.
6. In deriving the physical-domain bimaterial Green's functions, $x_3 \neq 0$ or $d \neq 0$ has been assumed. For the special case of $x_3 = d = 0$, i.e., both the field and source points are located on the interface for the bimaterial case or on the surface for the half-space case, the Green's functions presented above need to be modified. A detailed discussion is given in Appendix A. As can be observed, the interfacial Green's displacement has an expression similar to that derived by Barnett and Lothe (1975). Furthermore, the surface Green's displacement can be reduced to the real-form line-integral expression derived by Barnett and Lothe (1975) and recently by Wu (1998).

6. Numerical examples

In this section, several numerical examples are carried out to compare the present Green's functions and the existing analytical solutions for the isotropic or transversely isotropic half-space, and to evaluate the accuracy and the efficiency of the current solutions. Next, four cases are examined to demonstrate the effect of material anisotropy on the Green's displacements and stresses for anisotropic half-space and anisotropic bimaterials. For the isotropic or transversely isotropic half-space, the full-space Green's function employed is that derived by Pan and Chou (1976). While for anisotropic half-space and anisotropic bimaterials, the full-space Green's functions involved were evaluated using the explicit expression of Tonon et al. (1999).

Table 2
Surface Green's functions results in an isotropic half-space at $S(0, 0, 0)$, $F(a, -a, 0)$

$\boldsymbol{u}/(f/Ea)$	Present	Mindlin (1936)
(1, 1) = (2, 2)	0.248715	0.248712
(3, 3)	0.204826	0.204822
(1, 2) = (2, 1)	−0.0438818	−0.0438904
(1, 3) = −(3, 1)	0.0413854	0.0413803
−(2, 3) = (3, 2)	0.0413854	0.0413803
$\boldsymbol{\sigma}/(f/a^2)$		
(2, 2) = −(1, 1)	0.0956579	0.0956586
(2, 1) = −(1, 2)	0.0506308	0.0506428
(1, 6) = −(2, 6)	0.0731475	0.0731507
(3, 6)	−0.0318355	−0.0318310

6.1. Green's functions in a transversely isotropic or isotropic half-space

When the material in a half-space is either isotropic or transversely isotropic with the axis of symmetry being normal to the surface of the half-space, analytical Green's functions can be derived (Mindlin, 1936; Pan and Chou, 1979a, 1979b). To verify the current Green's functions, the Young's modulus $E = 1$ Msi, and the Poisson's ratio $\nu = 0.3$ for the isotropic case are selected. For the transversely isotropic case, the material properties selected are $E = 1$ Msi, $E' = 10$ Msi, $\nu = \nu' = 0.3$, $G' = 1$ Msi. Where E and E' are the Young's moduli in the plane of isotropy (x_1–x_2 plane) and the plane normal to it; ν and ν' are Poisson's ratios characterizing the lateral strain response in the plane of isotropy to a stress acting parallel and normal to it; and G' is the shear modulus in the plane normal to the plane of isotropy. The normalized numerical results of the half-space Green's functions, obtained with a 20-point Gauss quadrature for some source (S) and field (F) locations, are presented in Tables 1–3 and compared with the analytical Green's functions. In these tables, the first and second numbers in the bracket denote the force direction and the Green's function component, respectively. The second index in the stress $\boldsymbol{\sigma}$ (1, 2, 3, 4, 5) corresponds to the stress components (11, 22, 33, 23, 31). It is also noted that for the transversely isotropic half-space case (Table 3), the analytical Green's function results are obtained from a well-tested program (Pan, 1997). The present results in Table 2 are obtained using the surface Green's displacements and stresses derived in Appendix A; other results are from the reduced half-space expressions of Eqs. (34) and (37). Note also that the material properties need to be

Table 3
Green's functions results in a transversely isotropic half-space

$\boldsymbol{u}/(f/Ed)$	$S(0, 0, d)$, $F(0, 0, 0.75d)$		$S(0, 0, d)$, $F(0, 0, 1.25d)$	
	Present	Pan (1997)	Present	Pan (1997)
(1, 1) = (2, 2)	0.64233732	0.64233732	0.62325126	0.62325126
(3, 3)	0.39504886	0.39504886	0.37803374	0.37803374
$\boldsymbol{\sigma}/(f/d^2)$				
(1, 5) = (2, 4)	1.34601664	1.34601664	−1.43706520	−1.43706520
(3, 1) = (3, 2)	−0.65825908	−0.65825908	0.63970644	0.63970644
(3, 3)	11.9102536	11.9102536	−12.6181400	−12.6181400

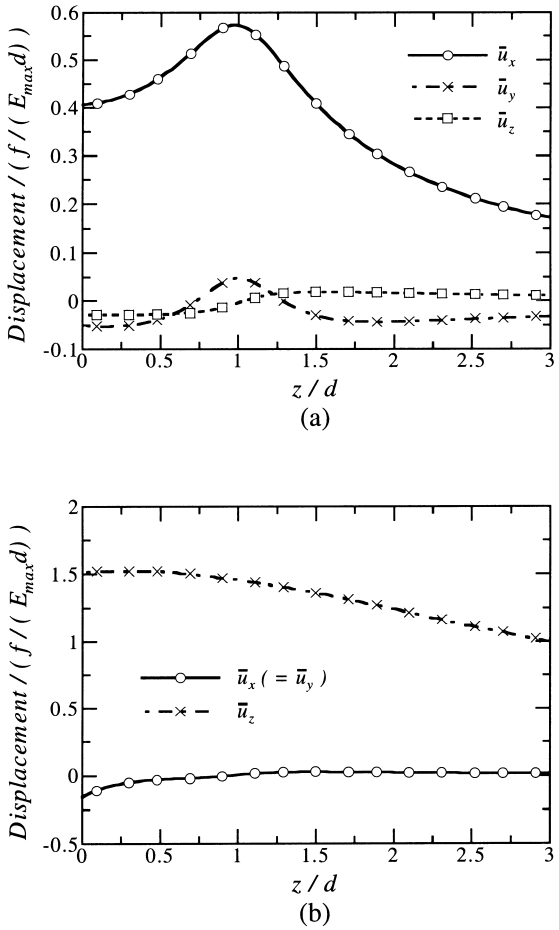

Fig. 2. The normalized Green's displacements in a half-space with NASA fabric. (a) $\boldsymbol{f} = (f_1, 0, 0)$; (b) $\boldsymbol{f} = (f_3, 0, 0)$.

slightly perturbed so that the requirement of distinct p_α can be met. As can be observed clearly from these tables, the numerical results from the current Green's functions are in excellent agreement with the existing analytical half-space Green's functions.

The bimaterial Green's functions for the case of isotropy or transverse isotropy are also tested. The Green's function results are also in good agreement with those shown in Guzina and Pak (1999) for the isotropic bimaterial case and in Yue (1995) for the transversely isotropic bimaterial case.

6.2. Green's functions in anisotropic half-spaces and bimaterials

After testing our Green's functions for the isotropic or transversely isotropic case, we now present the numerical analysis for some Green's function results in anisotropic half-spaces and anisotropic bimaterials. Two anisotropic (orthotropic) materials with a total of four cases are considered.

One of the orthotropic materials, named NASA fabric, is the composite material made by stacking layers of a carbon warp-knit fabric that was stitched with Kevlar-29 thread prior to introducing 3501-6

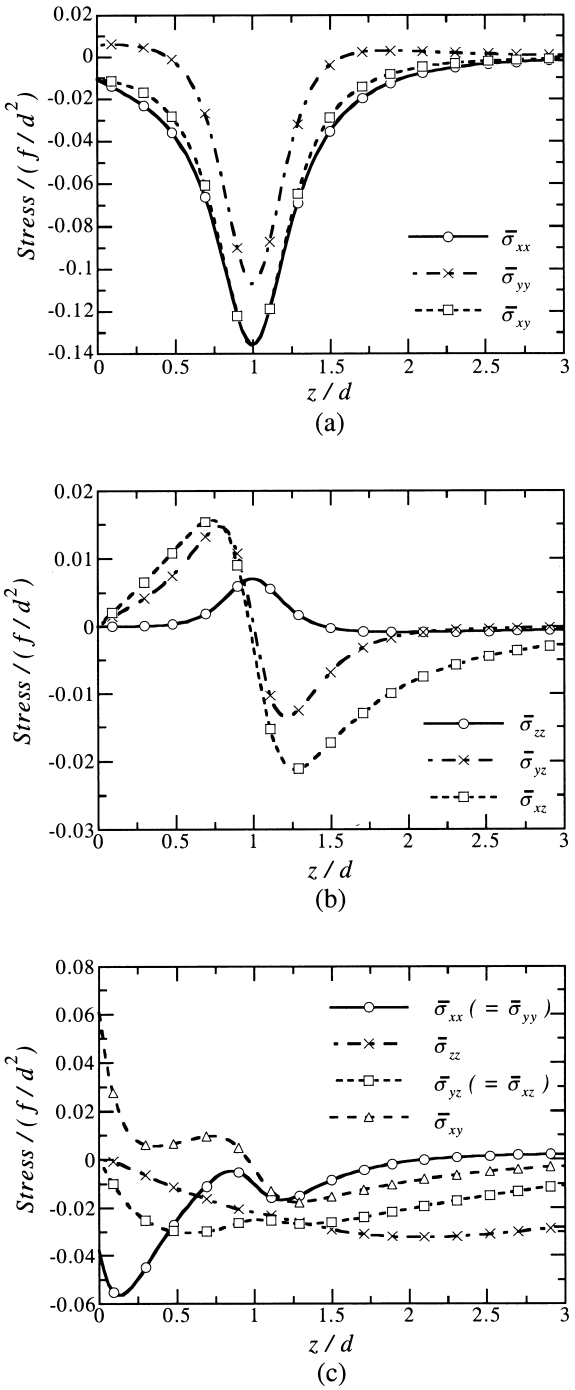

Fig. 3. The normalized Green's stresses in a half-space with NASA fabric. (a) and (b) $\boldsymbol{f} = (f_1, 0, 0)$; (c) $\boldsymbol{f} = (f_3, 0, 0)$.

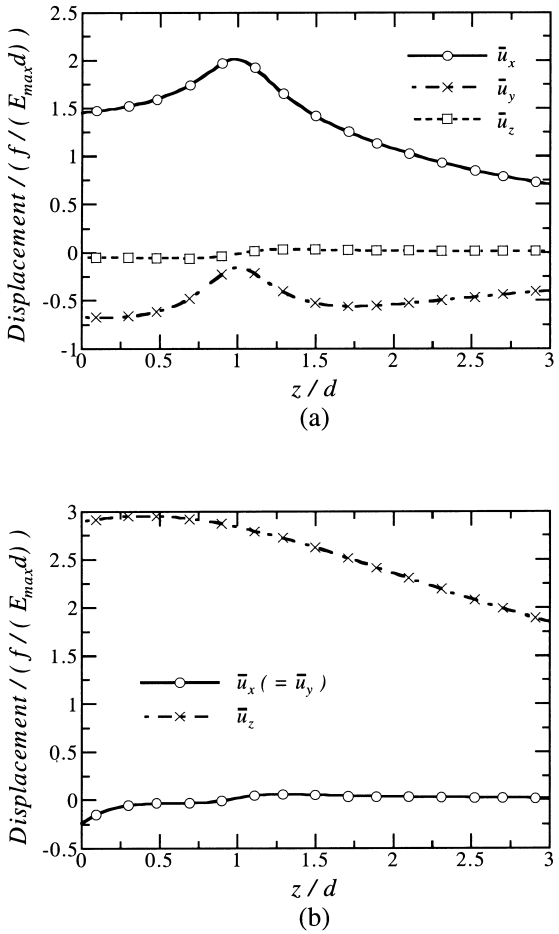

Fig. 4. The normalized Green's displacements in a half-space with graphite/epoxy. (a) $\boldsymbol{f} = (f_1, 0, 0)$; (b) $\boldsymbol{f} = (f_3, 0, 0)$.

epoxy resin (Pan and Yuan, 1999). The resin was introduced in an autoclave using a resin film infusing process. In the NASA Advanced Composites Transport Program, Boeing is using this material to develop a composite wing box for a transport aircraft. The resulting orthotropic material properties are:

$$E_X = 11.773 \text{ Msi}, \quad E_Y = 5.162 \text{ Msi}, \quad E_Z = 1.53 \quad \text{Msi},$$

$$G_{XY} = 2.479 \quad \text{Msi}, \quad G_{XZ} = 0.64 \text{ Msi}, \quad G_{YZ} = 0.57 \text{ Msi},$$

$$\nu_{XY} = 0.401, \quad \nu_{XZ} = 0.22, \quad \nu_{YZ} = 0.29.$$

The other one is a graphite/epoxy composite with stronger material anisotropy. The material properties are listed as follows:

$$E_X = 21.321 \text{ Msi}, \quad E_Y = 1.320 \text{ Msi}, \quad E_Z = 1.440 \text{ Msi},$$

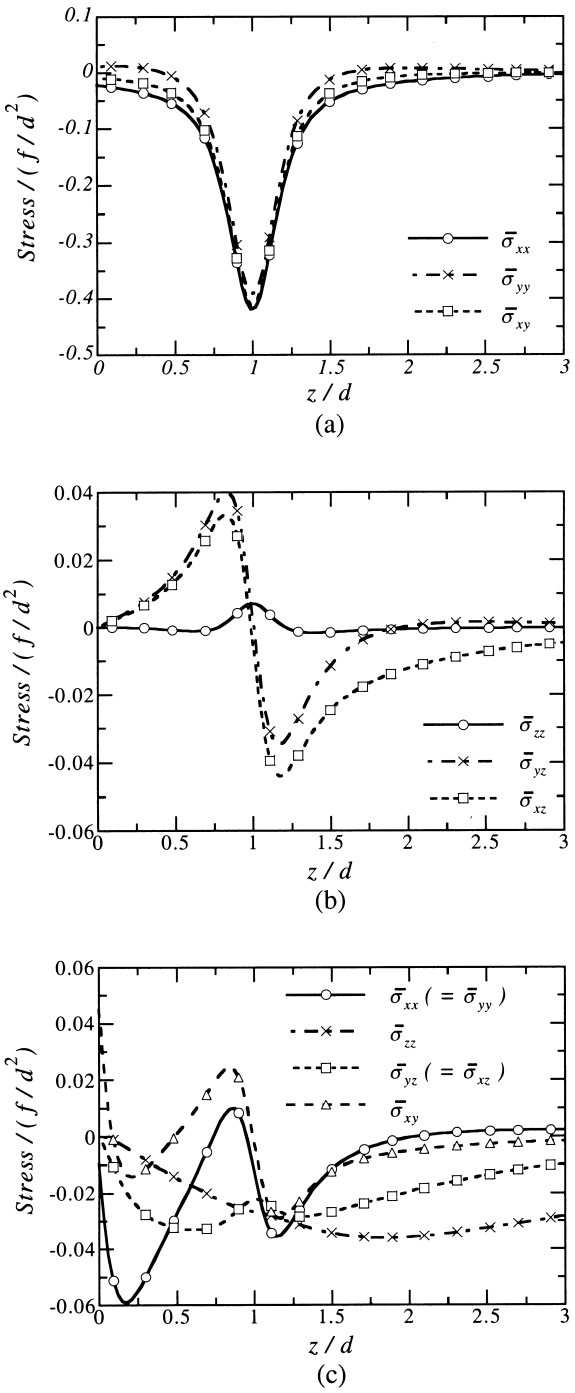

Fig. 5. The normalized Green's stresses in a half-space with graphite/epoxy. (a) and (b) $\boldsymbol{f} = (f_1, 0, 0)$; (c) $\boldsymbol{f} = (f_3, 0, 0)$.

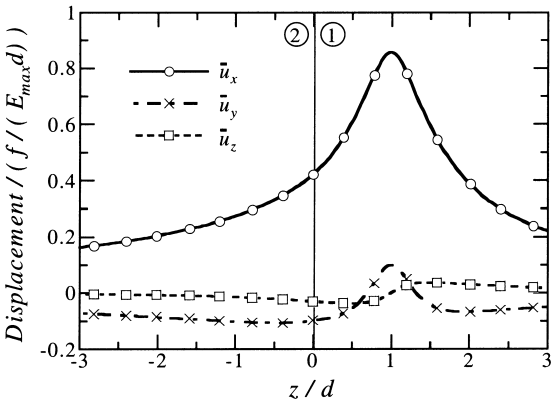

(a)

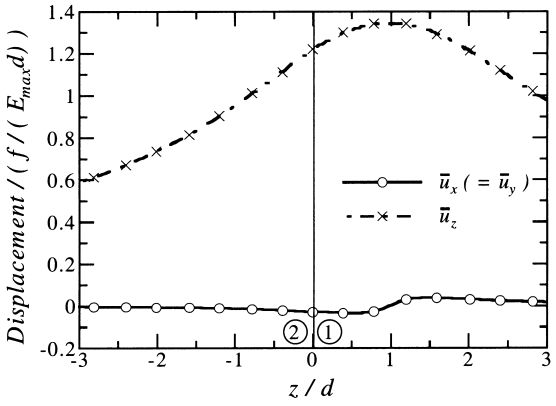

(b)

Fig. 6. The normalized Green's displacements in bimaterials with NASA fabric in material 1 and graphite/epoxy in material 2. (a) $\boldsymbol{f} = (f_1, 0, 0)$; (b) $\boldsymbol{f} = (f_3, 0, 0)$.

$$G_{XY} = 0.860 \text{ Msi}, \quad G_{XZ} = 0.619 \text{ Msi}, \quad G_{YZ} = 0.680 \text{ Msi},$$

$$\nu_{XY} = 0.3, \quad \nu_{XZ} = 0.3, \quad \nu_{YZ} = 0.49.$$

For the two composites, the principal material axes (E_X and E_Y) originally coincide with the x_1–x_2 axes. In the numerical calculation, the composites are oriented 45° counterclockwise with respect to the x_1-axis. Thus, the stiffness tensor C_{ijkl} of both materials in the structural coordinates (x_1, x_2, x_3) is monoclinic with symmetry plane at $x_3 = 0$. The four cases considered here are:

Case I: A half-space with NASA fabric material;
Case II: A half-space with graphite/epoxy;
Case III: Bimaterials with NASA fabric in material 1 and graphite/epoxy in material 2;
Case IV: Bimaterials with graphite/epoxy in material 1 and NASA fabric in material 2.

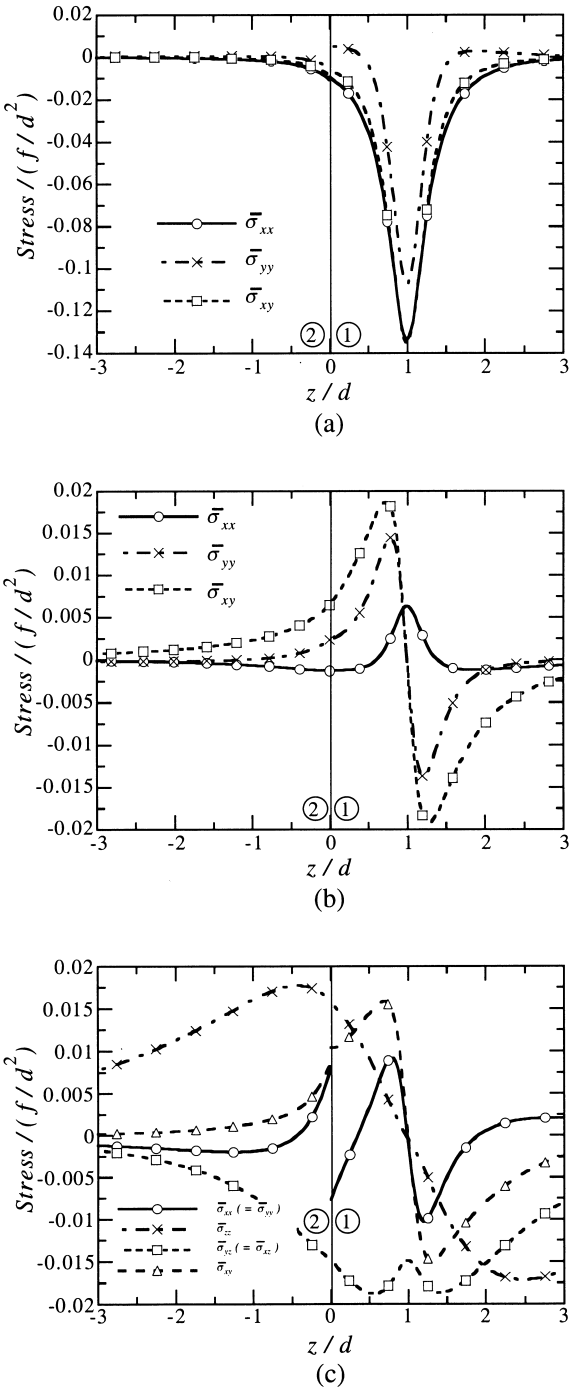

Fig. 7. The normalized Green's stresses in bimaterials with NASA fabric in material 1 and graphite/epoxy in material 2. (a) and (b) $\boldsymbol{f} = (f_1, 0, 0)$; (c) $\boldsymbol{f} = (f_3, 0, 0)$.

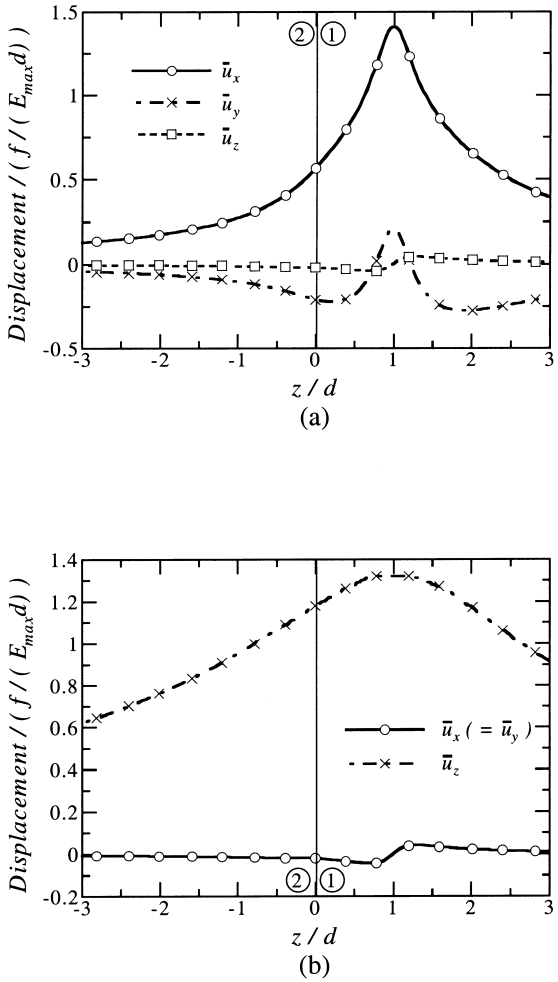

Fig. 8. The normalized Green's displacements in bimaterials with graphite/epoxy in material 1 and NASA fabric in material 2. (a) $\boldsymbol{f} = (f_1, 0, 0)$; (b) $\boldsymbol{f} = (f_3, 0, 0)$.

The normalized Green's displacements and stresses are presented in Figs. 2–9. In these figures, the point force (or source point) is applied at (0, 0, d). The displacements and stresses are plotted at field points $(x_1/d, x_2/d, x_3/d) = (1, 1, z/d)$ with z/d varying from 0 to 3 for Cases I and II; from -3 to 3 for Cases III and IV. In the figures where the displacements are shown, the Young's modulus $E_{\max} = 11.773$ Msi for Case I and $E_{\max} = 21.321$ Msi for other cases are used as a normalization parameter. It is also noted that, because of the special locations of the source and field points being investigated, the Green's functions due to a point force in the x_2-direction can be readily obtained from those due to a point force in the x_1-direction. Therefore, only the results caused by a point force the x_1- and x_3-directions are presented.

The normalized Green's displacements and stresses in anisotropic half-spaces (Cases I and II) are shown in Figs. 2–5. By comparing the normalized Green's displacements in NASA fabric half-space (Fig. 2(a) and (b)) with those in graphite/epoxy half-space (Fig. 4(a) and (b)), it is observed that the

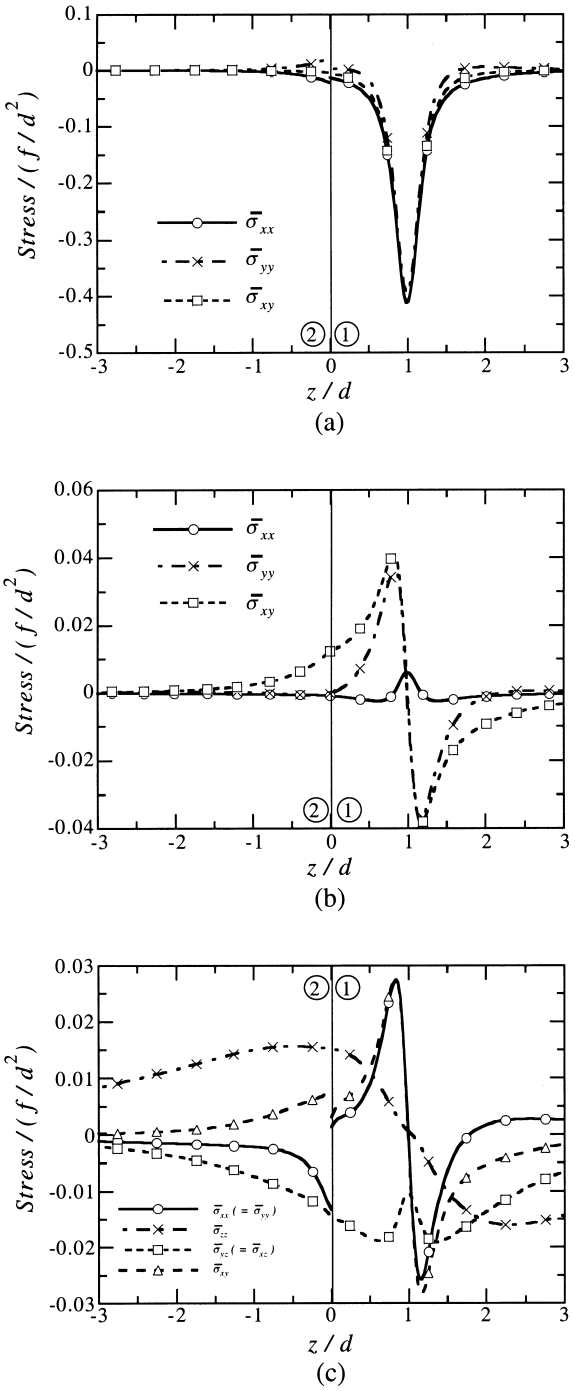

Fig. 9. The normalized Green's stresses in bimaterials with graphite/epoxy in material 1 and NASA fabric in material 2. (a) and (b) $\boldsymbol{f} = (f_1, 0, 0)$; (c) $\boldsymbol{f} = (f_3, 0, 0)$.

variations of the same Green's displacement components with respect to the x_3-coordinate are similar to each other. However, their magnitudes are different with those in graphite/epoxy half-space being larger. Similar conclusions can also be drawn by examining the variation of the corresponding Green's stresses (Fig. 3(a)–(c) for Case I and Fig. 5(a)–(c) for Case II). While the stresses caused by the point force in the x_3-direction have the same magnitude for these two cases, the magnitudes of the stresses caused by the point force in the x_1-direction in graphite/epoxy are larger than those in NASA fabric, especially for the in-plane stress components (Fig. 5(a) vs. Fig. 3(a)).

The normalized Green's displacements and stresses in anisotropic bimaterials are shown in Fig. 6. Again, the variations of the same Green's function components with respect to the x_3-coordinate are similar to each other. Similar trend to the half-space case, the magnitude of the in-plane stresses caused by the point force in the x_1-direction for Case IV (graphite/epoxy in material 1 and NASA fabric in material 2) is greater than those for Case III (NASA fabric in material 1 and graphite/epoxy in material 2) (Fig. 9(a) vs. 7(a)). Furthermore, the in-plane stresses experience a jump across the interface because of the discontinuity of the material property.

7. Conclusions

In this paper, three-dimensional Green's functions of point forces in anisotropic bimaterials are derived in terms of a regular line integral. Although the transformed-domain Green's functions are derived in exact closed-forms using the Stroh formalism, the explicit expressions for Green's functions in the physical domain are difficult to obtain due to the general anisotropy of the material and a geometry plane involved (e.g., surface plane for half-space case or interface plane for bimaterial case). The results from direct numerical calculation of the inverse Fourier transform may be inaccurate because of the infinite integral and singular kernels involved. The Fourier inverse transform using polar coordinate system is proposed to reduce the double infinite integrals to a finite line integral over $[0, 2\pi]$. Mindlin's superposition method (Mindlin, 1936) is also employed to handle the singularities in the bimaterial Green's functions so that the involved singularities appear only in the full-space Green's function that can be evaluated accurately using the explicit form expression (without numerical integral!). Therefore, the final physical bimaterial Green's functions are expressed as a sum of the explicit full-space Green's function and a complementary part. The complementary part of the bimaterial Green's functions is represented in terms of a regular line-integral that can be easily carried out by the regular numerical Gauss quadrature. In addition, derivatives of the complementary part of the Green's functions with respect to either the source or field point can be carried out exactly under the line integral. Some important features related to the bimaterial Green's functions, and their reduction to special cases have been discussed.

Numerical examples are given for both half-space and bimaterial cases with isotropic, transversely isotropic, and anisotropic material properties. For the half-space case with isotropic or transversely isotropic material properties, the current Green's function solutions are in excellent agreement with the existing analytical solutions. For the anisotropic case, the Green's functions in a half-space or in bimaterials show clearly the effect of material anisotropy on the displacement and stress distributions. The proposed method for calculating the Green's functions is very general and has proven to be effective and very accurate. The method can be used to derive Green's functions with higher derivatives if desired. The method will have wide applications to the boundary integral equation based method, and to the investigation of deformation, stress, and fracture analysis related to either anisotropic half-space or anisotropic bimaterials.

Acknowledgements

The authors would like to thank Prof. David Barnett of Stanford University for providing some updated references related to the three-dimensional anisotropic Green's functions and for instructive suggestions. They would also like to thank Dr. Gary Cai of Structures Technology Inc. and Dr. C.Y. Wang of Schlumberger-Doll Research for helpful discussions. This project was supported by the AFOSR under Grant No. F33615-97-C-5089.

Appendix A. Green's functions on the interface of bimaterials or the surface of a half-space

As discussed in the text, for the special case of $x_3 = d = 0$, i.e., both the field and source points are located on the interface for the bimaterial case or on the surface for the half-space case, the Green's functions need to be derived separately. It is emphasized here again that only for this special case, the singularities of the bimaterial or half-space Green's function occur in the complementary part of the solution. Fortunately however, these singularities are associated with one-dimensional finite-part integrals only, and therefore, can be calculated accurately in a similar way as the numerical Gauss quadrature. In the following, we choose the Green's displacement in material 1 for illustration. For this case, Eq. (34) is reduced to

$$\boldsymbol{u}_1(x_1, x_2, 0) = \boldsymbol{u}_1^{\infty}(x_1, x_2, 0) - \frac{i}{4\pi^2}\left[\int_0^{2\pi} \mathrm{d}\theta \int_0^{\infty} \bar{\boldsymbol{A}}_1 \boldsymbol{G}_1 \, \mathrm{e}^{-i\eta(x_1\cos\theta + x_2\sin\theta)} \boldsymbol{A}_1^{\mathrm{T}} \, \mathrm{d}\eta\right] \boldsymbol{f} \tag{A1}$$

Introducing the polar coordinate transform for the field point

$$x_1 = r\cos\theta_0$$

$$x_2 = r\sin\theta_0 \tag{A2}$$

and carrying out the integral with respect to η using relation (Barnett and Lothe, 1975)

$$\int_0^{\infty} \mathrm{e}^{-ikx} \, \mathrm{d}x = -\frac{i}{k} + \pi\delta(k) \tag{A3}$$

Eq. (A1) can be rewritten as

$$\boldsymbol{u}_1(x_1, x_2, 0) = \boldsymbol{u}_1^{\infty}(x_1, x_2, 0) - \frac{i}{4\pi^2}\left\{\int_0^{2\pi} \bar{\boldsymbol{A}}_1 \boldsymbol{G}_1 \boldsymbol{A}_1^{\mathrm{T}}\left[\frac{-i}{r\cos(\theta - \theta_0)} + \pi\delta(r\cos(\theta - \theta_0))\right] \mathrm{d}\theta\right\} \boldsymbol{f} \tag{A4}$$

By virtue of (Barnett and Lothe, 1975)

$$\delta(r\cos(\theta - \theta_0)) = \frac{\delta(\theta - \theta_0 \pm \pi/2)}{r|\sin(\theta - \theta_0)|} \tag{A5}$$

the interfacial Green's displacement in material 1 can be finally expressed as

$$\boldsymbol{u}_1(x_1, x_2, 0) = \boldsymbol{u}_1^{\infty}(x_1, x_2, 0) - \frac{1}{4\pi r}\left\{\frac{1}{\pi}\int_0^{2\pi} \frac{\bar{\boldsymbol{A}}_1 \boldsymbol{G}_1 \boldsymbol{A}_1^{\mathrm{T}}}{\cos(\theta - \theta_0)} \, \mathrm{d}\theta + i\left[\bar{\boldsymbol{A}}_1 \boldsymbol{G}_1 \boldsymbol{A}_1^{\mathrm{T}}\right]_{\theta = \theta_0 \pm \pi/2}\right\} \boldsymbol{f} \tag{A6}$$

with the integral being understood as the Cauchy principal value. If $\boldsymbol{G}_1$ is replaced by expression (31), this equation will then become the surface Green's displacement in an anisotropic half space. The Green's function expression can be further reduced to the surface Green's function obtained by Barnett and Lothe (1975) or recently by Wu (1998), i.e.,

$$\boldsymbol{u}(x_1, x_2, 0) = \frac{1}{2\pi r}\left[\boldsymbol{L}^{-1}[\theta_0] - \frac{1}{\pi}\int_0^{\pi} \frac{\boldsymbol{S}[\phi]\boldsymbol{L}^{-1}[\phi]}{\sin(\phi - \theta_0)}\,\mathrm{d}\phi\right]\boldsymbol{f} \tag{A7}$$

with $\phi = \theta + \pi/2$ (Barnett and Lothe, 1975; Ting, 1996). It is further noted that the interfacial Green's displacement can also be expressed in a real-form line-integral upon replacement of the involved complex matrices with real ones (Ting, 1996).

Similarly, the interfacial Green's traction vector in material 1 can be derived as

$$\boldsymbol{t}_1(x_1, x_2, 0) = \boldsymbol{t}_1^{\infty}(x_1, x_2, 0) + \frac{1}{4\pi r^2}\left\{\frac{1}{\pi}\int_0^{2\pi} \frac{\bar{\boldsymbol{B}}_1\boldsymbol{G}_1\boldsymbol{A}_1^{\mathrm{T}}}{\cos^2(\theta - \theta_0)}\,\mathrm{d}\theta \mp i\frac{\mathrm{d}[\bar{\boldsymbol{B}}_1\boldsymbol{G}_1\boldsymbol{A}_1^{\mathrm{T}}]}{\mathrm{d}\theta}|_{\theta=\theta_0\pm\pi/2}\right\}\boldsymbol{f} \tag{A8}$$

where the integral needs to be calculated in the finite-part sense (Paget, 1981).

Finally, the in-plane Green's stress vectors along the interface in materials 1 and 2 are obtained, respectively, as

$$\boldsymbol{s}_1(x_1, x_2, 0) = \boldsymbol{s}_1^{\infty}(x_1, x_2, 0) + \frac{1}{4\pi r^2}\left\{\frac{1}{\pi}\int_0^{2\pi} \frac{\bar{\boldsymbol{C}}_1\boldsymbol{G}_1\boldsymbol{A}_1^{\mathrm{T}}}{\cos^2(\theta - \theta_0)}\,\mathrm{d}\theta \mp i\frac{\mathrm{d}[\bar{\boldsymbol{C}}_1\boldsymbol{G}_1\boldsymbol{A}_1^{\mathrm{T}}]}{\mathrm{d}\theta}|_{\theta=\theta_0\pm\pi/2}\right\}\boldsymbol{f} \tag{A9}$$

$$\boldsymbol{s}_2(x_1, x_2, 0) = \frac{1}{4\pi r^2}\left\{\frac{-1}{\pi}\int_0^{2\pi} \frac{\boldsymbol{C}_2\boldsymbol{G}_2\boldsymbol{A}_1^{\mathrm{T}}}{\cos^2(\theta - \theta_0)}\,\mathrm{d}\theta \pm i\frac{\mathrm{d}[\boldsymbol{C}_2\boldsymbol{G}_2\boldsymbol{A}_1^{\mathrm{T}}]}{\mathrm{d}\theta}|_{\theta=\theta_0\pm\pi/2}\right\}\boldsymbol{f} \tag{A10}$$

References

Barnett, D.M., Lothe, J., 1975. Line force loadings on anisotropic half-spaces and wedges. Physica Norvegica 8 (1), 13–22.

Boussinesq, J., 1885. Applications des Potentiels a l'etude de l'equilibre et du mouvement des solids elastiques. Gauthier-Villars, Paris.

Dundurs, J., Hetenyi, M., 1965. Transmission of force between two semi-infinite solids. ASME, Journal of Applied Mechanics 32, 671–674.

Eshelby, J.D., Reed, W.T., Shockley, W., 1953. Anisotropic elasticity with applications to dislocation theory. Acta Metallurgica 1, 251–259.

Fares, N., 1987. Green's functions for plane-layered elastostatic and viscoelastic regions with application to 3D crack analysis. Ph.D. Thesis, M.I.T, USA.

Fares, N., Li, V.C., 1988. General image method in a plane-layered elastostatic medium. Journal of Applied Mechanics 55, 781–785.

Fredholm, I., 1900. Sur les equations de l'equilibre d'un corps solide elastique. Act Math 23, 1–42.

Gosling, T.J., Willis, J.R., 1994. A line-integral representation for the stresses due to an arbitrary dislocation in an isotropic half-space. Journal of the Mechanics and Physics of Solids 42 (8), 1199–1221.

Liao, J.J., Wang, C.D., 1998. Elastic solutions for a transversely isotropic half-space subjected to a point load. International Journal for Numerical and Analytical Methods in Geomechanics 22, 425–447.

Guzina, B.B., Pak, R.Y.S., 1999. Static fundamental solutions for a bi-material full-space. International Journal of Solids and Structures 36, 493–516.

Lifshitz, I.M., Rozenzweig, L.N., 1947. On the construction of the Green's tensor for the basic equation of the theory of elasticity of an anisotropic infinite medium. Zh. Eksp. Theo. Fiz 17, 783–791.

Mindlin, R.D., 1936. Force at a point in the interior of a semi-infinite solid. Physics 7, 195–202.
Mura, T., 1987. Micromechanics of Defects in Solids, 2nd ed. Martinus Nijhoff, Dordrecht, The Netherlands.
Paget, D.F., 1981. The numerical evaluation of Hadamard finite-part integrals. Numerische Mathematik 36, 447–453.
Pan, E., 1997. Static Green's functions in multilayered half spaces. Applied Mathematical Modelling 21, 509–521.
Pan, E., Yuan, F.G., 1999. Boundary element analysis of three-dimensional cracks in anisotropic solids. International Journal of Numerical Methods in Engineering, in press.
Pan, Y.C., Chou, T.W., 1976. Point force solution for an infinite transversely isotropic solid. ASME, Journal of Applied Mechanics 43, 608–612.
Pan, Y.C., Chou, T.W., 1979a. Green's function solutions for semi-infinite transversely isotropic materials. International Journal of Engineering Science 17, 545–551.
Pan, Y.C., Chou, T.W., 1979b. Green's functions for two-phase transversely isotropic materials. ASME, Journal of Applied Mechanics 46, 551–556.
Qu, J., Xue, Y., 1998. Three-dimensional interface cracks in anisotropic bimaterials: the non-oscillatory case. ASME, Journal of Applied Mechanics 65, 1048–1055.
Rongved, L., 1955. Force interior to one of two joined semi-infinite solids. In: Proc. 2nd Midwestern Conference on Solid Mechanics, 1–13.
Stroh, A.N., 1958. Dislocations and cracks in anisotropic elasticity. Philosophical Magazine 3, 625–646.
Stroh, A.N., 1962. Steady state problems in anisotropic elasticity. Journal of Mathematical Physics 41, 77–103.
Synge, J.L., 1957. The Hypercircle in Mathematical Physics. Cambridge University Press, Cambridge.
Thomson, W., (Lord Kelvin), 1848. Note on the integration of the equations of equilibrium of an elastic solid, Cambridge and Dublin Mathematical Journal, 76–99.
Ting, T.C.T., 1996. Anisotropic Elasticity. Oxford University Press, Oxford.
Ting, T.C.T., Lee, V.G., 1997. The three-dimensional elastostatic Green's function for general anisotropic linear elastic solids. The Quarterly Journal of Mechanics and Applied Mathematics 50, 407–426.
Tonon, F., Pan, E., Amadei, B., 1999. Green's functions and BEM formulation for 3D anisotropic media. Computers and Structures, in press.
Walker, K.P., 1993. Fourier integral representation of the Green's function for an anisotropic elastic half-space. Proceedings of the Royal Society of London A443, 367–389.
Walpole, L.J., 1996. An elastic singularity in joined half-spaces. International Journal of Engineering Science 34, 629–638.
Wang, C.Y., 1997. Elastic fields produced by a point source in solids of general anisotropy. Journal of Engineering Mathematics 32, 41–52.
Wang, C.D., Liao, J.J., 1999. Elastic solutions for a transversely isotropic half-space subjected to buried asymmetric-loads. International Journal for Numerical and Analytical Methods in Geomechanics 23, 115–139.
Willis, J.R., 1965. The elastic interaction energy of dislocation loops in anisotropic media. Quarterly Journal of Mechanics and Applied Mathematics 18, 419–433.
Wu, K.C., 1998. Generalization of the Stroh formalism to 3-dimensional anisotropic elasticity. Journal of Elasticity 51, 213–225.
Yu, H.Y., Sanday, S.C., 1991. Elastic fields in joined half-spaces due to nuclei of strain. Proceedings of The Royal Society of London A434, 503–519.
Yu, H.Y., Sanday, S.C., Rath, B.B., Chang, C.I., 1995. Elastic fields due to defects in transversely isotropic bimaterials. Proceedings of The Royal Society of London A449, 1–30.
Yuan, F.G., Yang, S., 1999. Three-dimensional Green's functions for composite laminates and composite half-space. Mechanics of Composite Materials and Structures, in press.
Yue, Z.Q., 1995. Elastic fields in two joined transversely isotropic solids due to concentrated forces. International Journal of Engineering Science 33, 351–369.